PNAS

Supplementary Information for

Hidden hotspots of amphibian biodiversity in China

Author

Wei Xu[1, #], Yun-He Wu[1, 2, #], Wei-Wei Zhou[1], Hong-Man Chen[1], Bao-Lin Zhang[1], Jin-Min Chen[1], Weihua Xu[3], Ding-Qi Rao[1], Haipeng Zhao[4], Fang Yan[1], Zhiyong Yuan[1], Ke Jiang[1], Jie-Qiong Jin[1], Mian Hou[5], Dahu Zou[1, 6], Li-Jun Wang[7], Yuchi Zheng[8], Jia-Tang Li[8], Jianping Jiang[8], Xiao-Mao Zeng[8], Youhua Chen[8], Zi-Yan Liao[8], Cheng Li[8], Xue-You Li[1], Wei Gao[1], Kai Wang[1, 2], Dong-Ru Zhang[1], Chenqi Lu[1, 9], Tingting Yin[1], Zhaoli Ding[1], Gui-Gang Zhao[1], Jing Chai[1], Wen-Ge Zhao[10], Ya-Ping Zhang[1], John J. Wiens[11, *], Jing Che[1, 2, *]

Affiliation

[1]Key Laboratory of Genetic Evolution and Animal Models, and Yunnan Key Laboratory of Biodiversity and Ecological Conservation of Gaoligong Mountain, Kunming Institute of Zoology, Chinese Academy of Sciences, Kunming, Yunnan 650223, China

[2]Southeast Asia Biodiversity Research Institute, Chinese Academy of Sciences, Yezin, Nay Pyi Taw 05282, Myanmar

[3]State Key Laboratory of Urban and Regional Ecology, Research Center for Eco-Environmental Sciences, Chinese Academy of Sciences, Beijing 100085, China

[4]School of Life Sciences, Henan University, Kaifeng, Henan 475004, China

[5]Institute of Continuing Education, Sichuan Normal University, Chengdu, Sichuan 610068, China

[6]College of Science, Tibet University, Lhasa, Tibet 850000, China

[7]School of Life Sciences, Hainan Normal University, Haikou, Hainan 571158, China

[8]Chengdu Institute of Biology, Chinese Academy of Sciences, Chengdu, Sichuan 610041, China

[9]Kunming College of Life Science, University of Chinese Academy of Sciences, Kunming 650204, China

[10]Department of Biology, College of Life and Environment Science, Harbin Normal University, Harbin 150080, China

[11]Department of Ecology and Evolutionary Biology, University of Arizona, Tucson, AZ 85721-0088, USA

#Authors contributed equally to this work

*Corresponding authors: Jing Che, John J. Wiens

Email: chej@mail.kiz.ac.cn; wiensj@arizona.edu

This PDF file includes:

Supplementary text
Figures S1 to S17
Tables S1 to S5
SI References

Other supplementary materials for this manuscript include the following (in separate files):

External Dataset S1. Species list of Chinese amphibians in this study. Names for potential cryptic species were combined by genus name, MOTU (molecular operational taxonomical unit) and sample ID. The divergence time, protection status, threat status, and endemism (non-endemic, endemic to China, or narrowly endemic) for each species is also listed.

External Dataset S2. Results of species-delimitation analyses. The haplotypes from the *COI* gene were estimated by DnaSP (see *SI Appendix*, Methods). Haplotypes were then analyzed using three species delimitation methods (GMYC, ABGD, mPTP). All cryptic species were named by genus name, MOTU and sample ID. Each family of Chinese amphibians was analyzed separately.

External Dataset S3. GenBank accession number of all gene sequences used for phylogeny reconstruction.

External Dataset S4. Maximum-likelihood tree for Chinese amphibians and relatives.

External Dataset S5. Time-calibrated tree used for estimating phylogenetic diversity and phylogenetic endemism among Chinese amphibians.

External Dataset S6. Concatenated alignments used for estimating the maximum-likelihood tree.

External Dataset S7. Ultrametric and non-ultrametric trees used for species delimitation in each family.

External Dataset S8. Species richness, endemism, phylogenetic diversity, and phylogenetic endemism of each grid cell.

Supplementary text

Methods

Phylogeny Estimation

We estimated a species-level, time-calibrated phylogeny that included most Chinese amphibian species, in order to calculate spatial patterns of phylogenetic diversity and phylogenetic endemicity. However, the higher-level relationships and divergence times in the tree were constrained based on previous phylogenomic studies (i.e., relationships among families), and our analysis primarily estimated relationships and divergence times within and among Chinese genera. The goal was not to provide a new, global-scale amphibian phylogeny.

We selected 12 nuclear genes (*BDNF*, *C-MYC*, *CXCR4*, *H3A*, *NCX1*, *POMC*, *RAG1*, *RAG2*, *RHOD*, *SIA*, *SLC8A3*, and *TYR*) and 7 mitochondrial genes (12S rRNA, 16S rRNA, *COI*, *CYTB*, *ND1*, *ND2*, and *ND3*) for estimating the phylogeny. These genes were selected because they were widely used in large-scale phylogenetic studies of amphibians (1–3). The molecular dataset included 521 described Chinese amphibian species, 100 potential cryptic Chinese species, and 1,057 non-Chinese species (External Dataset S3). These closely related non-Chinese species were included to increase the accuracy of estimated relationships among Chinese species, but were pruned out of the tree when calculating phylogenetic diversity and phylogenetic endemism for each grid cell in China (since they do not contribute to phylogenetic diversity and endemism in China). These closely related species included congeners of the Chinese amphibian species with available molecular data in GenBank, 1–2 species of other genera in the 13 families containing Chinese amphibians, and 1–2 species of other families of non-Chinese amphibians. Species were selected that had the most complete data for the 19 targeted genes. We used the same non-amphibian outgroups used in Hime et al. (4), including *Anolis carolinensis*, *Chrysemys picta*, *Gallus gallus*, *Homo sapiens*, and *Latimeria chalumnae*.

All sequences were aligned using MAFFT (5), which is integrated in FasParser 2.0 (6). Aligned sequences were then manually inspected for accuracy. We translated nucleotide sequences to amino acids for protein-coding regions, ensuring that an open reading frame was maintained. Given their stem and loop secondary structures, the 12S and 16S rRNA sequences were aligned using accuracy-oriented methods in MAFFT (G-IIS-i, L-INS-i, and E-INS-i) with slow speed but higher accuracy. The protein-coding genes were aligned by automatically selecting an appropriate strategy in MAFFT (from among L-INS-i, FFI-NS-i, and FFT-NS-2), according to the size of the dataset. A maximum-likelihood phylogeny was inferred with IQ-TREE v2.1.2 (7) using the UFBoot2 ultrafast bootstrapping (8) and SH-aLRT (9) options. We provided IQ-TREE with initially defined data blocks corresponding to three codon positions for each protein-coding gene and the full length for ribosomal genes (12S and 16S rRNA). IQ-TREE determined the optimal partitioning scheme (Table S3) by implementing ModelFinder (10) and automatically specified the best-fit model for all the partitions (Table S3).

We included a backbone family-level tree obtained from Portik et al. (11) and Hime et al. (4) to constrain the relationships between families and among the three major clades of amphibians. We extracted one species per family of anurans from the phylogeny of Portik et al. (11) using the R package *ape* (12), keeping only the topology and excluding branch-length information. We also extracted one species per family of caudates and gymnophionans from the phylogeny of Hime et al. (4), along with one species to represent Anura and five outgroup species. These two topologies were then combined to form a single topology representing all amphibian families. The topology from Portik et al. (11) was grafted manually into the Anura position in the phylogeny of Hime et al. (4), with anuran and caudates constrained as sister

groups. The combined topology was input into IQ-Tree in order to constrain higher-level relationships within the estimated species-level phylogeny.

The optimal tree inferred from IQ-TREE was then used in estimating divergence times with treePL v. 1.0 (13). treePL is an implementation of the penalized likelihood method (14) for very large datasets. Penalized likelihood (14) uses a tree with branch lengths and age constraints without prior parametric distributions. We utilized treePL because most other approaches to estimating divergence times (e.g., the uncorrelated lognormal relaxed clock approach in BEAST; 15) would not be practical given the large number of taxa analyzed here. Rather than using fossil calibration points, we used the results of recent large-scale studies (4, 11) to constrain the divergence times among families and the three major amphibian clades. These constraints were put in the configuration file of treePL. Specifically, we set the minimum and maximum divergence times among families and major clades to equal the estimated age for each of these clades, using Portik et al. (11) for anurans and Hime et al. (4) for caudates, gymnophionans, and the major amphibian clades. The treePL analysis was primed to determine optimal settings, and the tree was then time-calibrated with the thorough setting. We tested eight potential smoothing parameters (0.0001, 0.001, 0.01, 0.1, 1, 10, 100, 1,000). The best-fit smoothing parameter was 0.0001. The final maximum-likelihood tree and the final time-calibrated tree are available as External Datasets S4 and S5, respectively. The final concatenated alignment is available as External Dataset S6. Given the constraints, the higher-level relationships and divergence times closely matched those estimated by Portik et al. (11) and Hime et al. (4).

Cryptic species estimation

We used molecular data to estimate the number of cryptic species present among China's amphibian species. A total of 2,306 individuals from 313 described species were sampled through our fieldwork in China, primarily from 2001–2020. Muscle or liver tissues taken from each individual collected were fixed in 95% ethanol. We performed morphological identifications according to the amphibian identification keys of Fei et al. (16). All specimens were initially assigned to a described, morphology-based species. Data were obtained from all individuals from the mitochondrial cytochrome oxidase (*COI*) gene. Sequences were generated following laboratory procedures and primers described by Che et al. (17). All newly obtained sequences were deposited in GenBank (External Dataset S2). We also downloaded 5,177 additional *COI* sequences from 352 described species in GenBank for China's amphibian species and their congeners (downloaded by the end of 2020). A total of 212 species overlapped between GenBank and our new data here. However, we added sequences for 101 described species that were not previously deposited on GenBank. In total, our dataset included 7,483 *COI* sequences from 453 described Chinese amphibian species, corresponding to an overall coverage of 81.3% (453/557) of described amphibian species known to occur in China by 2020 (External Dataset S2). The remaining 18.7% of described species lacked *COI* data, which precluded analysis of their potential cryptic species. We followed the taxonomy of AmphibiaChina (18) from December, 2020. Specimen details, including voucher numbers, GenBank accession numbers, and species-delimitation results are provided in External Dataset S2. Research protocols were approved by the Ethics Committee of the Kunming Institute of Zoology, Chinese Academy of Science (IACUC No.: IACUC-OE-2022-07-001).

To identify potential cryptic species, we estimated haplotype phylogenies for each of the amphibian families that occur in China except Cryptobranchidae (see below). We used DnaSP 6

(19) to generate haplotypes for *COI* sequences of each family separately (i.e., individuals with identical haplotypes were amalgamated).

We then employed three species-delimitation methods: (i) the Automatic Barcode Gap Discovery (ABGD) method (20), (ii) the General Mixed Yule Coalescent (GMYC) approach (21), and (iii) the Multi-rate Poisson Tree Processor (mPTP) method (22). We describe how we integrated results from the three approaches below. Each method has somewhat different requirements. The ABGD method requires only haplotype sequences as input. The GMYC approach requires an ultrametric tree. The mPTP method requires a phylogenetic tree with branch lengths. Consequently, we utilized BEAST (15) and MrBayes (23) to generate ultrametric and non-ultrametric trees (respectively) for each family, based on their haplotype sequences.

The ultrametric tree for each family was estimated using the uncorrelated lognormal relaxed molecular-clock model in BEAST 1.8.0 (15). We used the GTR + gamma substitution model, treating the *COI* gene as a single partition. Markov chains were run for 100 million generations, sampling every 10,000th generation. TRACER 1.7 was used to confirm when the output reached stationarity (effective sample size >200 for all variables; 24). We initially used fewer generations and utilized TRACER to evaluate the effective sample size, incrementing the number of generations if stationarity was not achieved. Ultimately, we used 100 million generations in for each family to ensure that all of them reached stationarity. Majority-rule consensus trees were generated using TREEANNOTATOR 1.4.5 (15). Note that each tree was ultrametric but not time calibrated, and therefore we did not utilize any external calibration points.

The non-ultrametric tree for each family was estimated using MrBayes 3.2.7a (23). We used the GTR + gamma model with a single partition. The Markov Chains Monte Carlo (MCMC) chains were run for 10 million generations and sampled every 1,000 generations with a burn-in of 25%. Both BEAST and MrBayes were implemented using the CIPRES web server (25). These ultrametric and non-ultrametric trees are available in External Dataset S7.

Three species-delimitation methods (GMYC, ABGD, mPTP) were applied to each family to infer potential species, also referred to as Molecular Operational Taxonomic Units (MOTUs; 26). These three methods are widely used for species delimitation with single-locus data (27). The ultrametric tree generated from BEAST for each family was used as input in a single-threshold GMYC analysis in the R package *splits* (28). We performed ABGD on the haplotype sequences utilizing an online platform (https://bioinfo.mnhn.fr/abi/public/abgd/abgdweb.html) with the default parameters. mPTP was performed on the mPTP webserver (http://mptp.h-its.org), using the non-ultrametric Bayesian tree (from MrBayes) for each family as input.

Empirical studies have shown that ABGD tends to undersplit species (29, 30), whereas GMYC and mPTP tend to oversplit species (29, 31). Combinations of different methods have been used to overcome these potential biases (27). The individual results of ABGD, mPTP, and GMYC are presented in detail in External Dataset S2.

Potential cryptic species were identified generally following Dincă et al. (32). Each of the morphology-based species included was classified into one of three categories: “Match”, “Cryptic species”, and “Merge." (i) Match: the morphology-based species was supported by the three methods as a single MOTU. (ii) Cryptic species: one or more of the species-delimitation methods inferred one or more cryptic species within the morphology-based species (i.e., the single morphology-based species contained two or more MOTUs). If the three methods agreed about the number of cryptic species present, then we used that number of potential cryptic species for further analyses. If the three methods disagreed on the number of cryptic species

present within a given morphology-based species then we conservatively utilized the smallest number of cryptic species inferred among the three methods (including cases in which one method inferred that no cryptic species were present in the morphology-based species and the other methods inferred one or more). (iii) Merge: the morphology-based species was assigned to the same MOTU as another morphology-based species by all three methods. There could be various reasons why two (or more) morphology-based species were assigned to the same MOTU, including a recent origin of these lineages, recent introgression of mitochondrial genes, or problematic morphology-based taxonomy (e.g., 33, 34). Therefore, to be conservative, we tentatively continued to recognize these morphology-based species for our analyses here. Note that the species limits (and cryptic species) inferred here were then used in the final time-calibrated tree among Chinese amphibians.

Using combinations of methods to delimit cryptic species has been recommended (e.g., 27, 35–38). However, given that the putative cryptic species identified here were based only on mitochondrial DNA, we considered these to be only potential cryptic species. These potential species should be further investigated with multiple nuclear markers. Many case studies have found mismatch between species limits from mitochondrial DNA and multi-locus nuclear DNA (e.g., 39), but there does not seem to be a consensus as to whether mitochondrial DNA consistently underestimates or overestimates true species numbers. We tried to be conservative here, by using only the minimum estimated number of cryptic species within a morphology-based species and by not lumping morphology-based species based on mitochondrial data alone.

We had *COI* data for 453 Chinese amphibian species, but there were an additional 104 described species (stopping by the end of 2020) for which we lacked *COI* data. It was important to make sure that the inferred cryptic species did not belong to these described species to avoid counting the same species twice in our biodiversity analyses. This determination was made by initially assigning each potential cryptic species to a morphology-based described species. Although we did not have *COI* data for every described species, none of the potential cryptic species should belong to those unsampled described species, based on our initial morphological identifications. Thus, we conclude that none of the 90 inferred cryptic species belonged to any of these 104 described morphology-based species. To further test the validity of these cryptic species, we extracted the divergence time of each cryptic species and described species of Chinese amphibians from the full tree based on the combined nuclear and mitochondrial data. We then performed a Wilcoxon rank-sum test in R to determine if there was a statistically significant difference between the mean ages of each set of species. If no significant difference was found, it would suggest that these cryptic species are similar in age to the described species, providing further support for their validity. Conversely, if the cryptic species were significantly younger, this would suggest that they are less genetically distinct than described species.

Biogeographic regionalization

We estimated major biogeographic regions based on dissimilarity between each pair of grid cells. Traditionally, China has been divided into seven zoogeographic regions based on expert opinion (40): Northeast China, North China, Northwest China, Xizang Plateau, Central China, Southwest China, and South China. Here, biogeographical regions were delineated among the focal 567 grid cells based on Simpson's dissimilarity index (β_{sim}; 41). This index measures pairwise dissimilarity in species composition among grid cells. β_{sim} is robust to changes in species richness and can efficiently discriminate species turnover from nestedness (42). We estimated β_{sim} between each pair of grid cells as follows:

$$\beta_{sim}=1-\frac{S_{ab}}{\min(S_a,S_b)+S_{ab}}$$

where S_{ab} is the number of species that co-occur in these two grid cells, and S_a and S_b are the number of species unique to each grid cell. Estimation was performed using the R package *vegan* 43).

We applied the unweighted pair-group method using arithmetic averages (UPGMA) to the dissimilarity matrix (44). A UPGMA dendrogram displays relationships among grid cells and has good performance across datasets (44). We then used the *GMD* package in R (45) to determine optimal K clusters on the UPGMA dendrogram. A suitable cut-off point was chosen based on the best K value.

Results

Summary of cryptic species estimation

Overall, the species-delimitation analyses conservatively estimated 90 cryptic species among the 453 described Chinese species with *COI* data (External Dataset S2; Table S4). We identified 73 potential cryptic species from our new *COI* sequence data and another 17 potential cryptic species from published *COI* sequences. Among the 90 cryptic species identified (External Dataset S2), 27 cryptic species were consistent with other studies that applied species-delimitation methods to 16S rRNA data (*Megophrys* and *Leptobrachella*; 46–48; *Rhacophorus rhodopus*, 49) and to 16S rRNA, *COI*, and *ND2* data (*Amolops*; 50).

In addition to these 90 cryptic species identified here, 10 cryptic species reported by previous studies were also included in our analysis (External Dataset S1). For example, six cryptic species within *Andrias davidianus* (Cryptobranchidae) were identified by both genomic data and mtDNA markers, including *COI* sequences (51). We estimated the total number of morphologically cryptic species in China (not described before the end of 2020) to be 100 (External Dataset S2; Table S4). We also found that 14 morphology-based Chinese species were inferred to be conspecific with other morphology-based species based on these analyses (labeled as "Merge" in the External Dataset S2; Table S4). However, we do not support synonymizing these species without additional testing.

We found potential cryptic species of Chinese amphibians in all families except for Bombinatoridae, Ceratobatrachidae, Hylidae, Hynobiidae, and Ichthyophiidae (External Dataset S2; Table S4). The most cryptic diversity was found in Megophryidae with 56 cryptic species (56.0% of all cryptic species). There were 31 cryptic species in the genus *Megophrys* alone. Previous studies have also suggested the existence of many cryptic species in this genus (46, 48). The family with the second highest number of cryptic species was Ranidae (*n*=12 cryptic species). The other families with cryptic species were Rhacophoridae (*n*=10 cryptic species), Bufonidae (*n*=6), Salamandridae (*n*=6), Cryptobranchidae (*n*=6), Dicroglossidae (*n*=3), and Microhylidae (*n*=1).

Using the time-calibrated tree based on nuclear and mitochondrial data for all Chinese amphibians, we found no significant difference in mean ages of cryptic species and described species (6.94 Ma vs. 7.68 Ma; Wilcoxon rank sum test, *P*=0.2033; External Dataset 1). There was extensive overlap in the ages of the described and cryptic species (Fig. S1), strongly suggesting that the cryptic species inferred here tend to be roughly as divergent as described species.

Biogeographic regions

UPGMA clustering analysis of these 567 grid cells and 647 species identified eight large-scale biogeographic regions (Fig. S3a). These were different from the seven Chinese zoogeographic regions (Fig. S3b) defined by Zhang (40). In general, our results showed an increased number of regions delimited in western China, with fewer regions delimited in the east and north. Species richness (Fig. 2a), endemism (Fig. 2b), phylogenetic diversity (Fig. 2c) and phylogenetic endemism (Fig. 2d) were mapped on these grid cells. Among these regions, South China had exceptionally high species richness and phylogenetic diversity (Table S5). After correcting for the number of grid cells, the South Yunnan Mountains, Himalayas, Yunnan Plateau, Hengduan Mountains, and South China had higher richness than the other regions (Table S5). Areas with high endemism (Fig. 2b) and phylogenetic endemism (Fig. 2d) included South China, South Yunnan Mountains, Yunnan Plateau, and the Himalayas.

References

1. R. A. Pyron, J. J. Wiens, A large-scale phylogeny of Amphibia including over 2800 species, and a revised classification of extant frogs, salamanders, and caecilians. *Mol. Phylogenet. Evol.* **61**, 543–583 (2011).
2. R. A. Pyron, Biogeographic analysis reveals ancient continental vicariance and recent oceanic dispersal in amphibians. *Syst. Biol.* **63**, 779–797 (2014).
3. W. Jetz, R. A. Pyron, The interplay of past diversification and evolutionary isolation with present imperilment across the amphibian tree of life. *Nat. Ecol. Evol.* **2**, 850–858 (2018).
4. P. M. Hime *et al*., Phylogenomics reveals ancient gene tree discordance in the amphibian tree of life. *Syst. Biol.* **70**, 49–66 (2021).
5. K. Katoh, D. M. Standley, MAFFT multiple sequence alignment software version 7: improvements in performance and usability. *Mol. Biol. Evol.* **30**, 772–780 (2013).
6. Y. B. Sun, FasParser2: A graphical platform for batch manipulation of tremendous amount of sequence data. *Bioinformatics* **34**, 2493–2495 (2018).
7. B. Q. Minh *et al.*, IQ-TREE 2: new models and efficient methods for phylogenetic inference in the genomic era. *Mol. Biol. Evol.* **37**, 1530–1534 (2020).
8. D. T. Hoang, O. Chernomor, A. von Haeseler, B. Q. Minh, L. S. Vinh, UFBoot2: Improving the Ultrafast Bootstrap Approximation. *Mol. Biol. Evol.* **35**, 518–522 (2018).
9. S. Guindon *et al*., New algorithms and methods to estimate maximum-likelihood phylogenies: assessing the performance of PhyML 3.0. *Syst. Biol.* **59**, 307–321 (2010).
10. S. Kalyaanamoorthy, B. Q. Minh, T. K. F. Wong, A. von Haeseler, L. S. Jermiin, ModelFinder: fast model selection for accurate phylogenetic estimates. *Nat. Methods.* **14**, 587–589 (2017).
11. D. M. Portik, J. W. Streicher, J. J. Wiens, Frog phylogeny: A time-calibrated, species-level tree based on hundreds of loci and 5,242 species. *Mol. Phylogenet. Evol*. **188,** 107907 (2023).
12. E. Paradis, K. Schliep, ape 5.0: an environment for modern phylogenetics and evolutionary analyses in R. *Bioinformatics* **35**, 526–528 (2019).
13. S. A. Smith, B. C. O'Meara, treePL: Divergence time estimation using penalized likelihood for large phylogenies. *Bioinformatics* **28**, 2689–2690 (2012).
14. M. J. Sanderson, Estimating absolute rates of molecular evolution and divergence times: A penalized likelihood approach. *Mol. Biol. Evol.* **19**, 101–109 (2002).
15. A. J. Drummond, A. Rambaut, BEAST: Bayesian evolutionary analysis by sampling trees. *BMC Evol. Biol.* **7**, 1–8 (2007).
16. L. Fei et al., (2009) Fauna Sinica, Amphibia. Anura, vol. 2. Science Press, Beijing (in Chinese).
17. J. Che *et al.*, Universal *COI* primers for DNA barcoding amphibians. *Mol. Ecol. Resour.* **12**, 247–258 (2012).
18. AmphibiaChina, 2020. The database of China's amphibians. Electronic Database accessible at http://www.amphibiachina.org/. Kunming Institute of Zoology (CAS), Kunming, Yunnan, China.
19. J. Rozas *et al.*, DnaSP 6: DNA sequence polymorphism analysis of large data sets. *Mol. Biol. Evol.* **34**, 3299–3302 (2017).
20. N. Puillandre, A. Lambert, S. Brouillet, G. J. M. E. Achaz, ABGD, Automatic Barcode Gap Discovery for primary species delimitation. *Mol. Ecol.* **21**, 1864–1877 (2012).

21. J. Pons *et al.*, Sequence-based species delimitation for the DNA taxonomy of undescribed insects. *Syst. Biol.* **55**, 595–609 (2006).
22. P. Kapli *et al.*, Multi-rate Poisson tree processes for single-locus species delimitation under maximum likelihood and Markov chain Monte Carlo. *Bioinform.* **33**, 1630–1638 (2017).
23. F. Ronquist *et al.*, MrBayes 3.2: efficient Bayesian phylogenetic inference and model choice across a large model space. *Syst. Biol.* **61**, 539–542 (2012).
24. A. Rambaut, A. J. Drummond, D. Xie, G. Baele, M. A. Suchard, Posterior summarization in Bayesian phylogenetics using Tracer 1.7. *Syst. Biol.* **67**, 901–904 (2018).
25. M. A. Miller, W. Pfeiffer, T. Schwartz, Creating the CIPRES Science Gateway for inference of large phylogenetic trees. In: Gateway Computing Environments Workshop (GCE), IEEE, pp. 1–8 (2010).
26. M. Blaxter *et al.*, Defining operational taxonomic units using DNA barcode data. *Philos. Trans. R. Soc. B: Biol. Sci.* **360**, 1935–1943 (2005).
27. A. Luo, C. Ling, S. Y. Ho, C. D. Zhu, Comparison of methods for molecular species delimitation across a range of speciation scenarios. *Syst. Biol.* **67**, 830-846 (2018).
28. T. Ezard, T. Fujisawa, T. G. Barraclough (2009) splits: Species' Limits by Threshold Statistics. R package version 1.0-14/r31. http://R-Forge.R-project.org/projects/splits/.
29. M. Pentinsaari, R. Vos, M. Mutanen, Algorithmic single-locus species delimitation: effects of sampling effort, variation and nonmonophyly in four methods and 1870 species of beetles. *Mol. Ecol. Resour.* **17**, 393–404 (2017).
30. M. A. Renner, M. M. Heslewood, S. D. Patzak, A. Schäfer-Verwimp, J. Heinrichs, By how much do we underestimate species diversity of liverworts using morphological evidence? An example from Australasian *Plagiochila* (Plagiochilaceae: Jungermanniopsida). *Mol. Phylogenet. Evol.* **107**, 576–593 (2017).
31. A. Paz, A. J. Crawford, Molecular-based rapid inventories of sympatric diversity: a comparison of DNA barcode clustering methods applied to geography-based vs clade-based sampling of amphibians. *J. Biosci.* **37**, 887–896 (2012).
32. V. Dincă *et al.*, DNA barcode reference library for Iberian butterflies enables a continental-scale preview of potential cryptic diversity. *Sci. Rep.* **5**, 12395 (2015).
33. Y. H. Wu *et al.*, DNA barcoding of Chinese snakes reveals hidden diversity and conservation needs. *Mol. Ecol. Resour.* **23**, 1124-1141 (2023).
34. Y. Shen Y *et al.*, DNA barcoding the ichthyofauna of the Yangtze River: Insights from the molecular inventory of a mega-diverse temperate fauna. *Mol. Ecol. Resour.* **19**, 1278–1291 (2019).
35. M. Kekkonen, P. D. N. Hebert, DNA barcode-based delineation of putative species: Efficient start for taxonomic workflows. *Mol. Ecol. Resour.* **14**, 706–715 (2014).
36. M. Kekkonen, M. Mutanen, L. Kaila, M. Nieminen, P. D. N. Hebert, Delineating species with DNA barcodes: A case of taxon dependent method performance in moths. *PLoS One* **10**, e0122481 (2015).
37. Q. Li *et al.*, DNA barcoding subtropical aphids and implications for population differentiation. *Insects* **11**, 11 (2019).
38. G. Limmon *et al.*, Assessing species diversity of Coral Triangle artisanal fisheries: A DNA barcode reference library for the shore fishes retailed at Ambon harbor (Indonesia). *Ecol. Evol.* **10**, 3356–3366 (2020).

39. Z. Y. Yuan *et al.,* Historical mitochondrial genome introgression confounds species delimitation: evidence from phylogenetic inference in the *Odorrana grahami* species complex. *Curr. Zool*. **69**, 82–90 (2023).
40. R. Zhang, China animal geography. Science Press, Beijing (1999).
41. G. G. Simpson, Mammals and the nature of continents. *Am. J. Sci.* **241**, 1–31 (1943).
42. A. Baselga, Partitioning the turnover and nestedness components of beta diversity. *Glob. Ecol. Biogeogr.* **19**, 134–143 (2010).
43. J. Oksanen *et al.,* vegan: community ecology package. R package version 2.3-2 (2015).
44. H. Kreft, W. Jetz, A framework for delineating biogeographical regions based on species distributions. *J. Biogeogr.* **37**, 2029–2053 (2010).
45. X. Zhao, E. Valen, B. J. Parker, A. Sandelin, Systematic clustering of transcription start site landscapes. *PLoS One* **6**, e23409 (2011).
46. J. M. Chen *et al.,* A novel multilocus phylogenetic estimation reveals unrecognized diversity in Asian horned toads, genus *Megophrys* sensu lato (Anura: Megophryidae). *Mol. Phylogenet. Evol.* **106**, 28–43 (2017).
47. J. M. Chen *et al.,* Large-scale phylogenetic analyses provide insights into unrecognized diversity and historical biogeography of Asian leaf-litter frogs, genus *Leptolalax* (Anura: Megophryidae). *Mol. Phylogenet. Evol.* **124**, 162–171 (2018).
48. Z. Liu *et al.,* Prevalence of cryptic species in morphologically uniform taxa–Fast speciation and evolutionary radiation in Asian frogs. *Mol. Phylogenet. Evol.* **127**, 723–731 (2018).
49. K. O. Chan, L. L. Grismer, R. M. Brown, Comprehensive multi-locus phylogeny of Old World tree frogs (Anura: Rhacophoridae) reveals taxonomic uncertainties and potential cases of over- and underestimation of species diversity. *Mol. Phylogenet. Evol.* **127**, 1010–1019 (2018).
50. Y. H. Wu *et al.* A combined approach of mitochondrial DNA and anchored nuclear phylogenomics sheds light on unrecognized diversity, phylogeny, and historical biogeography of the torrent frogs, genus *Amolops* (Anura: Ranidae). *Mol. Phylogenet. Evol.* **148**, 106789 (2020).
51. F. Yan *et al.,* The Chinese giant salamander exemplifies the hidden extinction of cryptic species. *Curr. Biol.* **28**, R590–R592 (2018).
52. L. Revell, phytools 2.0: an updated R ecosystem for phylogenetic comparative methods (and other things). *PeerJ*. **12**, e16505 (2024).
53. O. Venter *et al.,* Sixteen years of change in the global terrestrial human footprint and implications for biodiversity conservation. *Nat. Commun.* **7**, 1–11 (2016).
54. J. Soubrier *et al.,* The influence of rate heterogeneity among sites on the time dependence of molecular rates. *Mol. Biol. Evol*. **29**, 3345–3358 (2012).

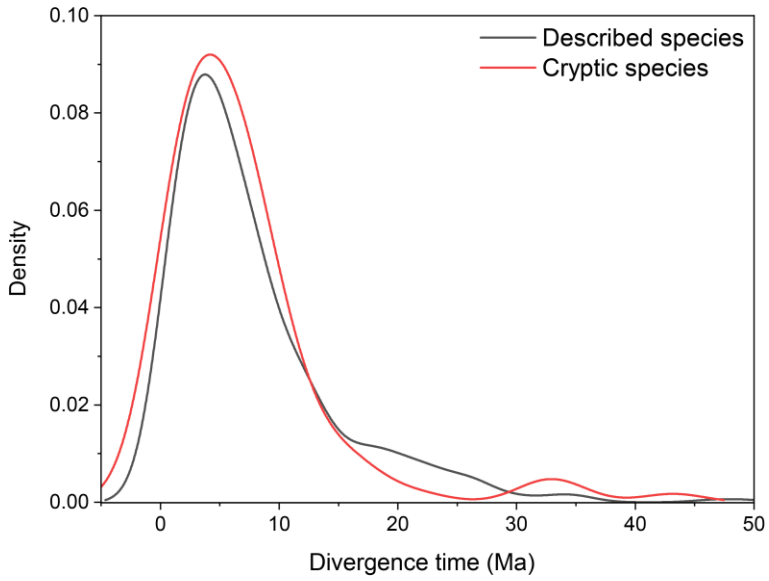

Fig. S1. Comparison of ages of described and cryptic species. This figure displays the kernel density of estimated ages of cryptic species (red) and described species (black) of Chinese amphibians. Ages for each species were extracted from the time-calibrated tree based on both nuclear and mitochondrial data. Data for each species are given in Dataset S1.

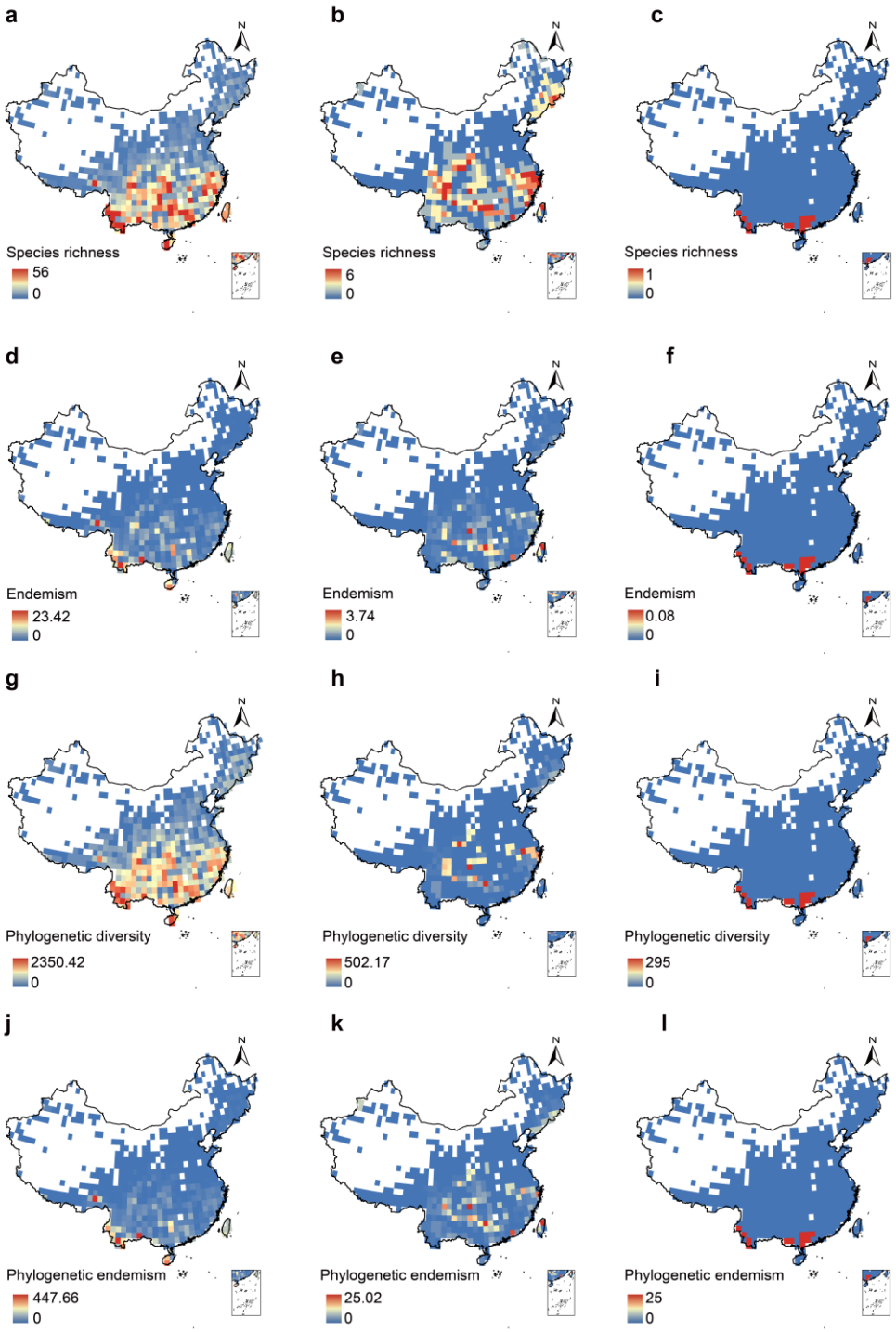

Fig. S2. Diversity patterns in Chinese amphibians shown separately for each of the three major clades. Patterns are shown for frogs (a, d, g, j) salamanders (b, e, h, k), and caecilians (c, f, i, l). Spatial patterns are shown for species richness (a–c), weighted species endemism (d–f), phylogenetic diversity (g–i), and phylogenetic endemism (j–l). The white grid cells lacked recorded amphibian species and were excluded from the analyses.

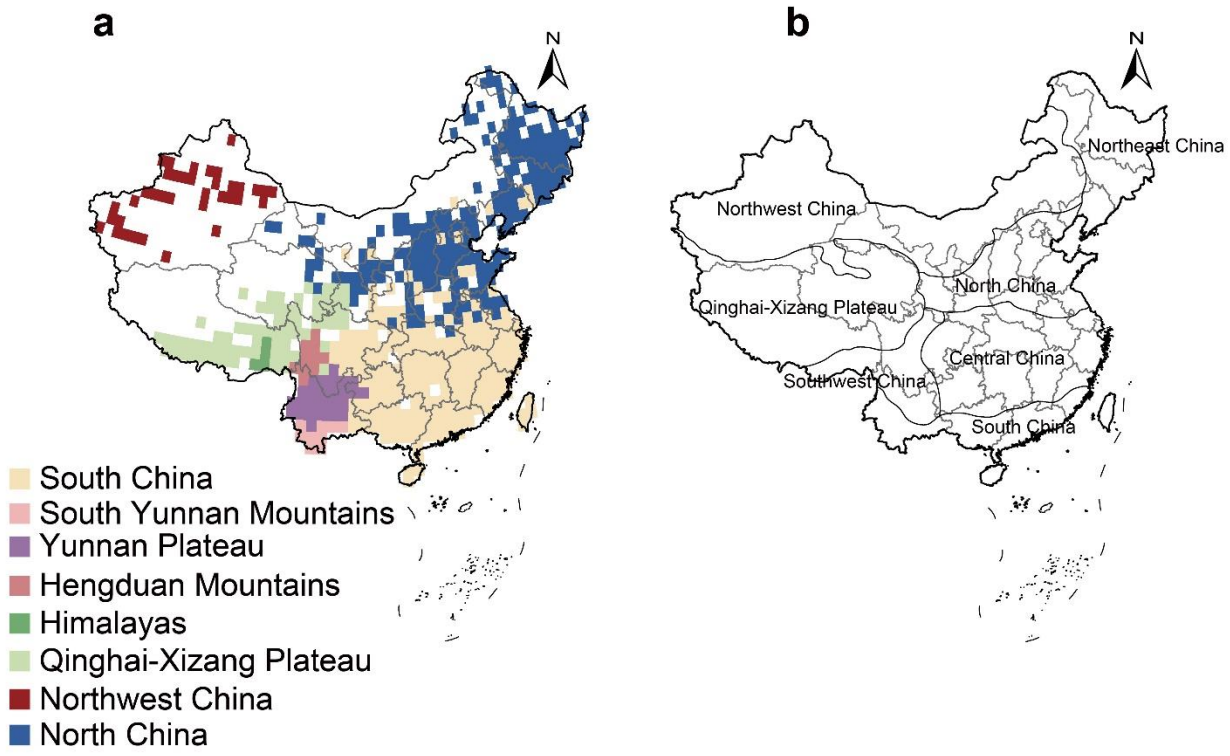

463

464 **Fig. S3. Eight biogeographic regions delimited by UPGMA clustering in this study (a) and**
465 **seven zoogeographic regions (b) modified from Zhang (40)**. The gray lines indicate the
466 provincial boundaries of China.
467

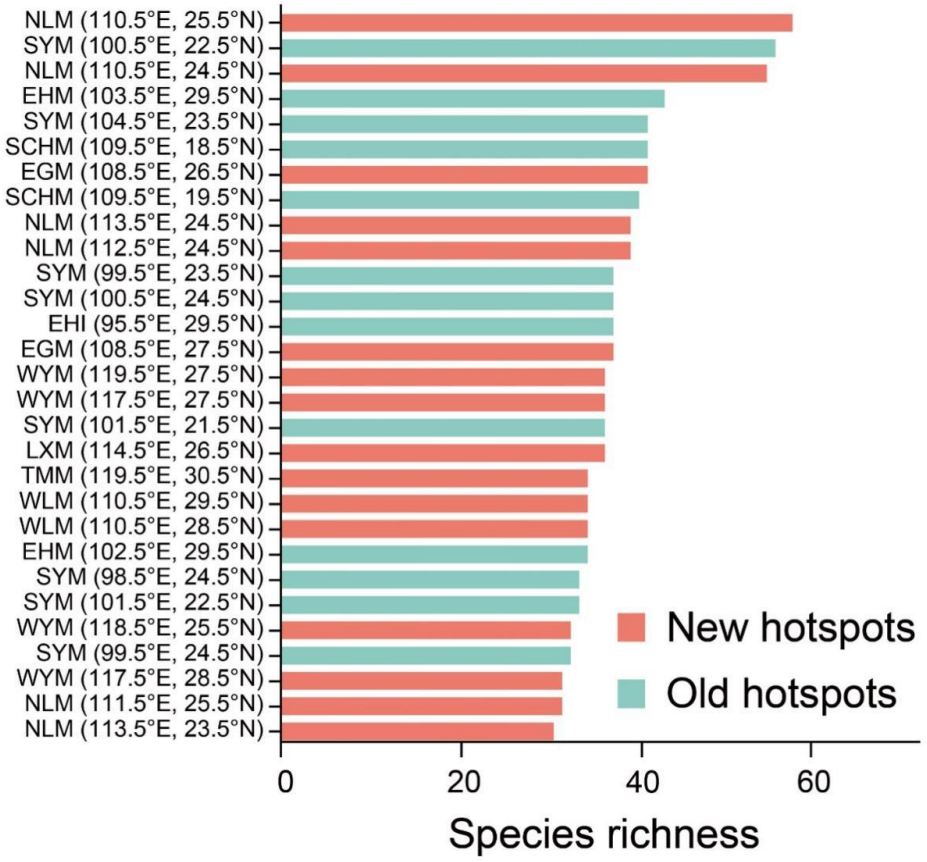

Fig. S4. Total species richness of each grid cell in the ten hotspots. The longitude and latitude of the centroid of each grid cell are shown in the brackets. The 10 geographically distinct biodiversity hotspots are: Eastern Himalayas (EHI), Eastern Hengduan Mountains (EHM), Southwest Yunnan Mountains (SYM), South-Central Hainan Mountains (SCHM), Nanling Mountains (NLM), Wuling Mountains (WLM), Eastern Guizhou Mountains (EGM), Luoxiao Mountains (LXM), Wuyi Mountains (WYM), and Tianmu Mountains (TMM).

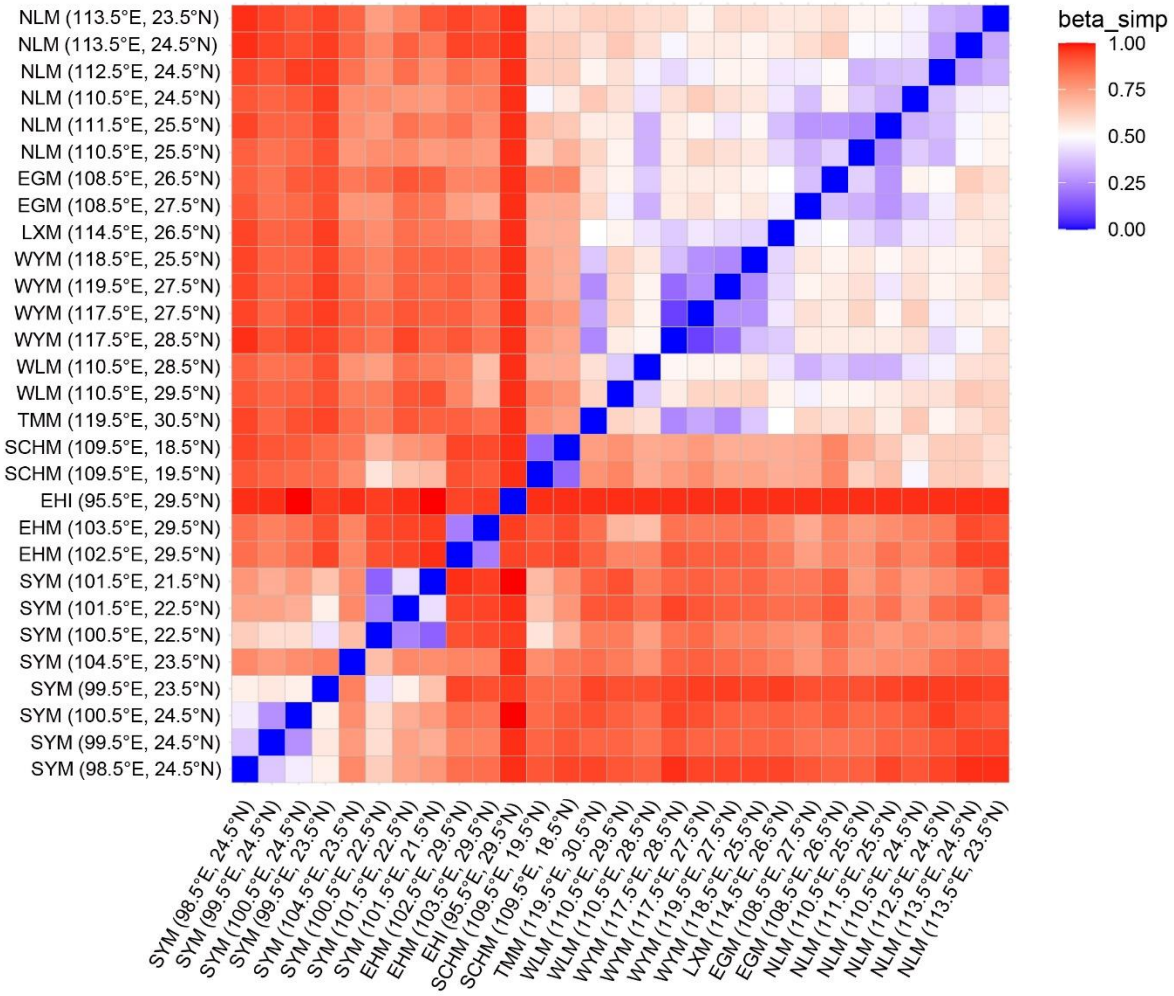

Fig. S5. Beta-Simpson values for each of the 29 most species rich grid cells. Higher values indicate larger differences in species composition between pairs of grid cells. The name of each grid cell consists of the abbreviation of the hotspot it is contained in and the longitude and latitude of the center of the grid cell. The 10 hotspots are: EHI: Eastern Himalayas (old hotspots), EHM: Eastern Hengduan Mountains (old hotspot), SYM: Southwest Yunnan Mountains (old hotspot), SCHM: South-Central Hainan Mountains (old hotspot), NLM: Nanling Mountains (new hotspot), WLM: Wuling Mountains (new hotspot), EGM: Eastern Guizhou Mountains (new hotspots), LXM: Luoxiao Mountains (new hotspot), WYM: Wuyi Mountains (new hotspots), TMM: Tianmu Mountains (new hotspot).

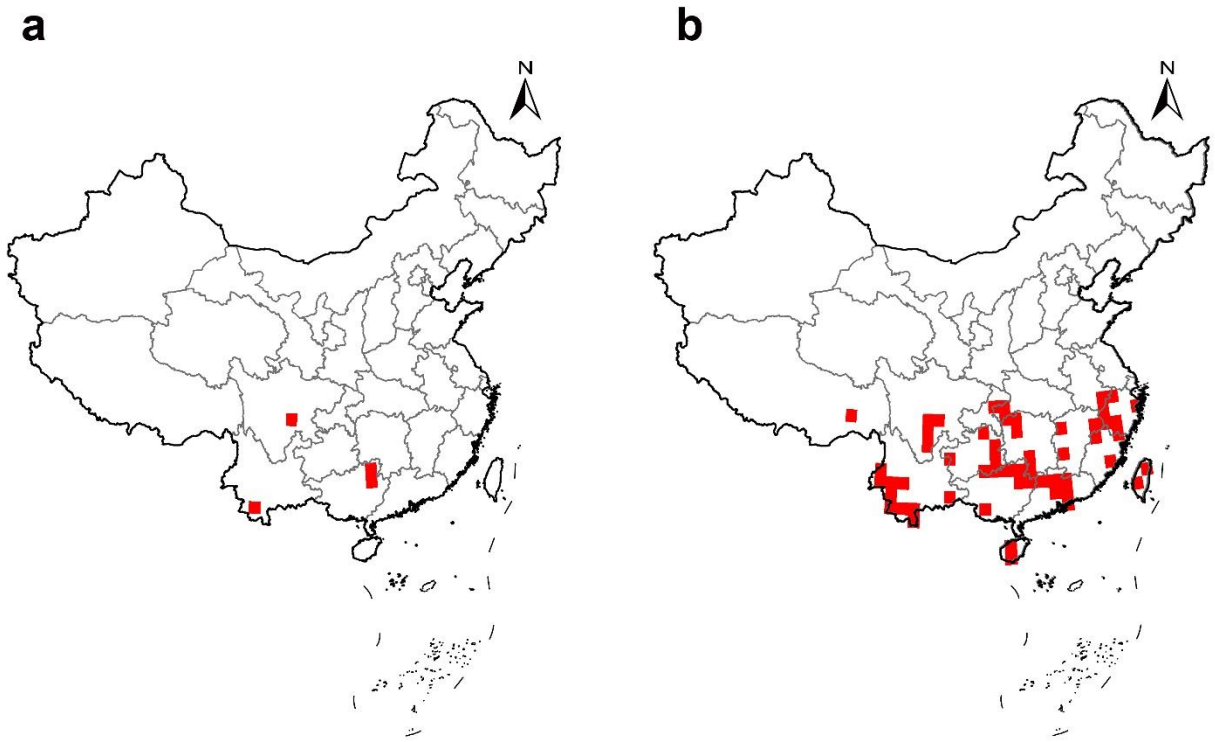

Fig. S6. The most species-rich grid cells under two alternative thresholds. The red color shows the most species-rich grid cells based on the upper 99th percentile for species richness (a), and the 90th percentile (b). The gray lines indicate the provincial boundaries of China.

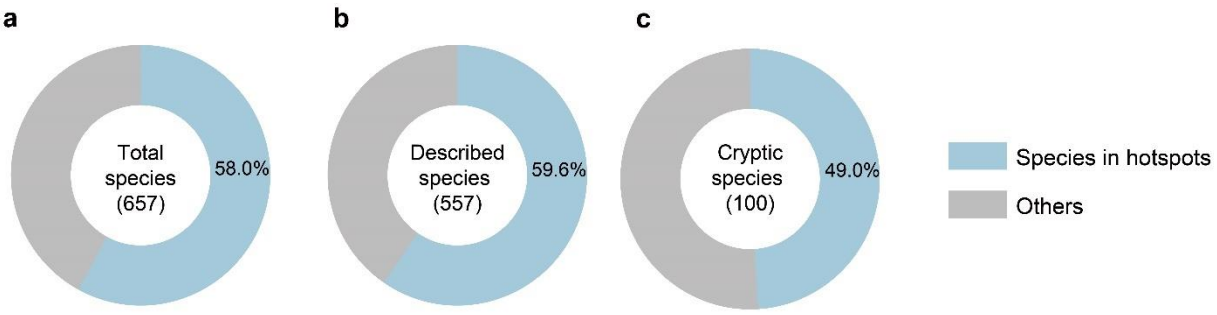

Fig. S7. Distribution of species among hotspot and non-hotspot grid cells. (a) Total species. (b) Described species. (c) Cryptic species.

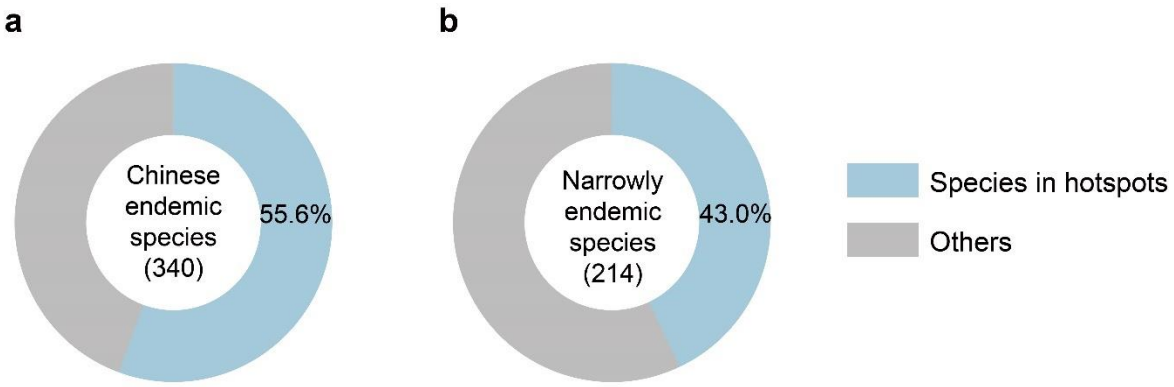

Fig. S8. Distribution of endemic Chinese species among hotspot and non-hotspot grid cells. (a) Species endemic to China. (b) Narrowly endemic species (distribution limited to a single grid cell).

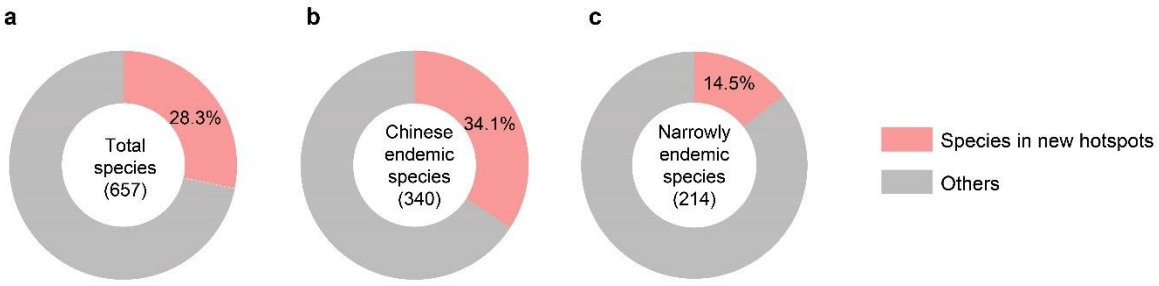

505
506
507 **Fig. S9. Distribution of species among the six new hotspots and other areas.**

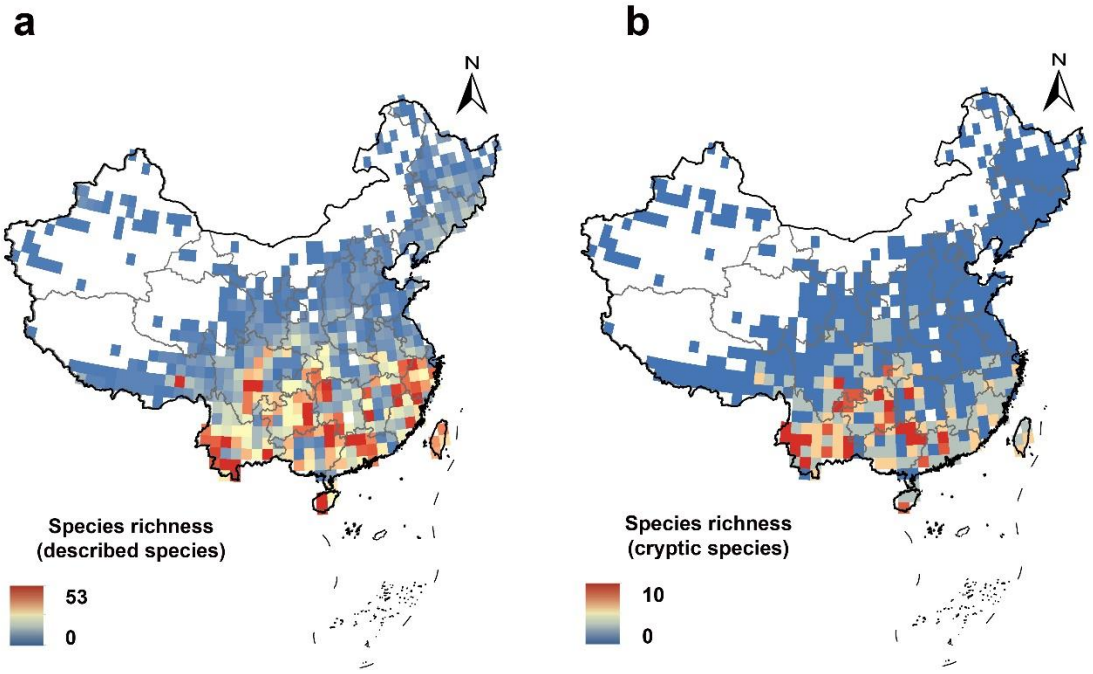

Fig. S10. Spatial richness patterns of described species (a) and cryptic species (b). The gray lines indicate the provincial boundaries of China.

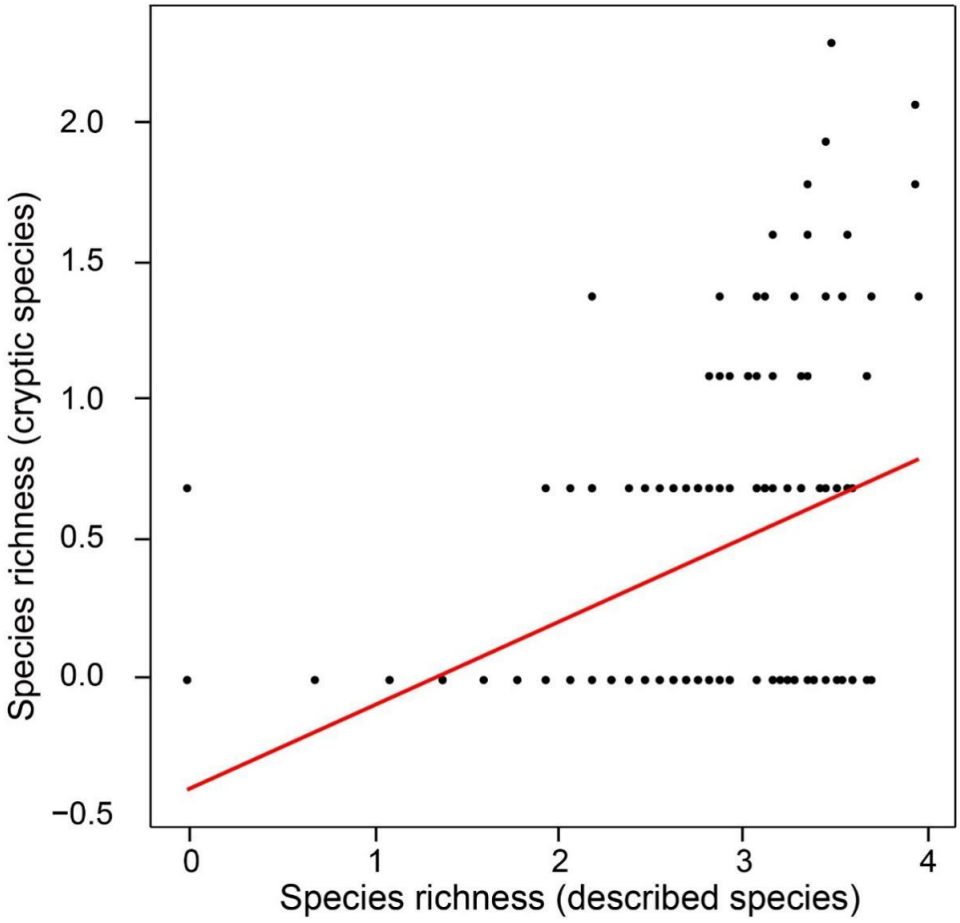

Fig. S11. Ordinary least squares (OLS) linear regression between species richness of described species (ln-transformed) and cryptic species (ln-transformed) among the 567 grid cells. The result showed these two variables had a significant, positive relationship (r^2=0.49; p<0.0001). The regression after spatial autocorrelation also supports the significant positive relationship (estimates=0.46, z value= 5.15, p<0.0001).

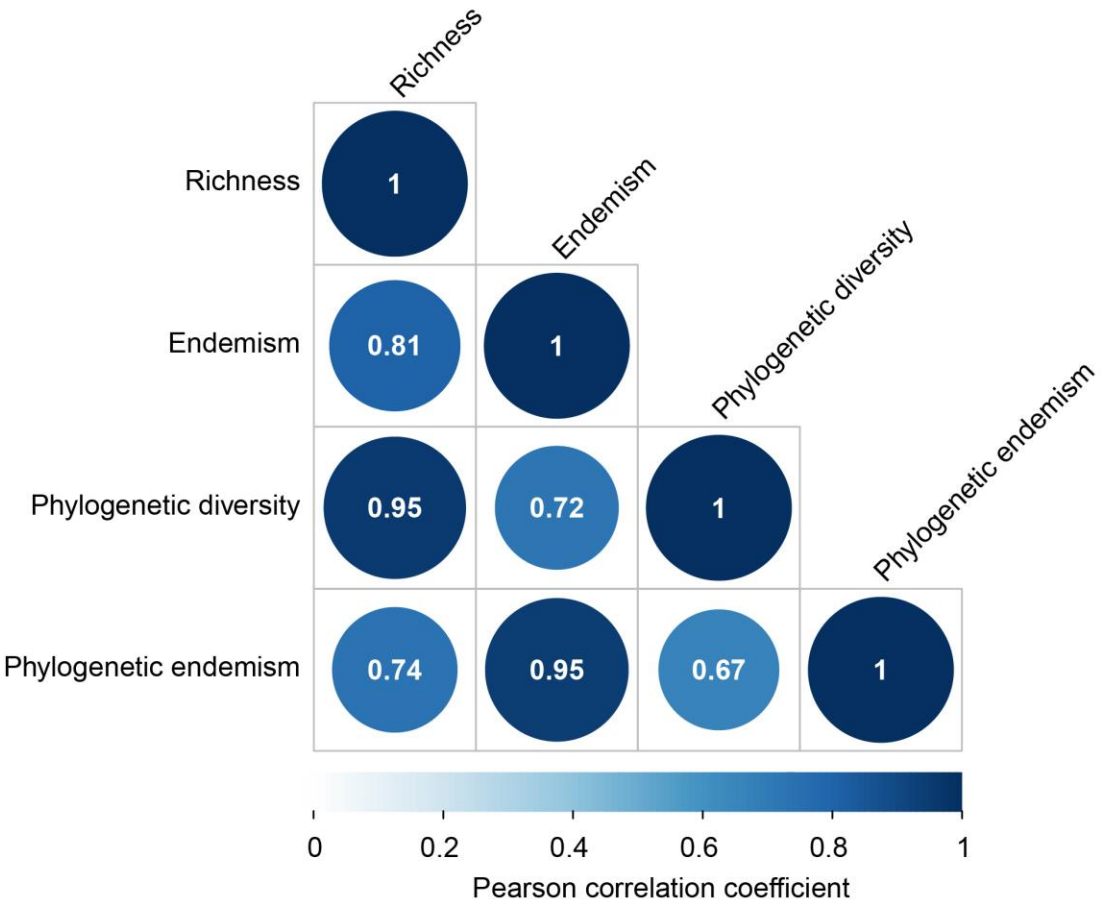

Fig. S12. Correlations between different diversity metrics. The Pearson correlation coefficients were calculated among grid cells for each pair of variables: species richness, endemism, phylogenetic diversity, and phylogenetic endemism. Darker blues indicate stronger correlations.

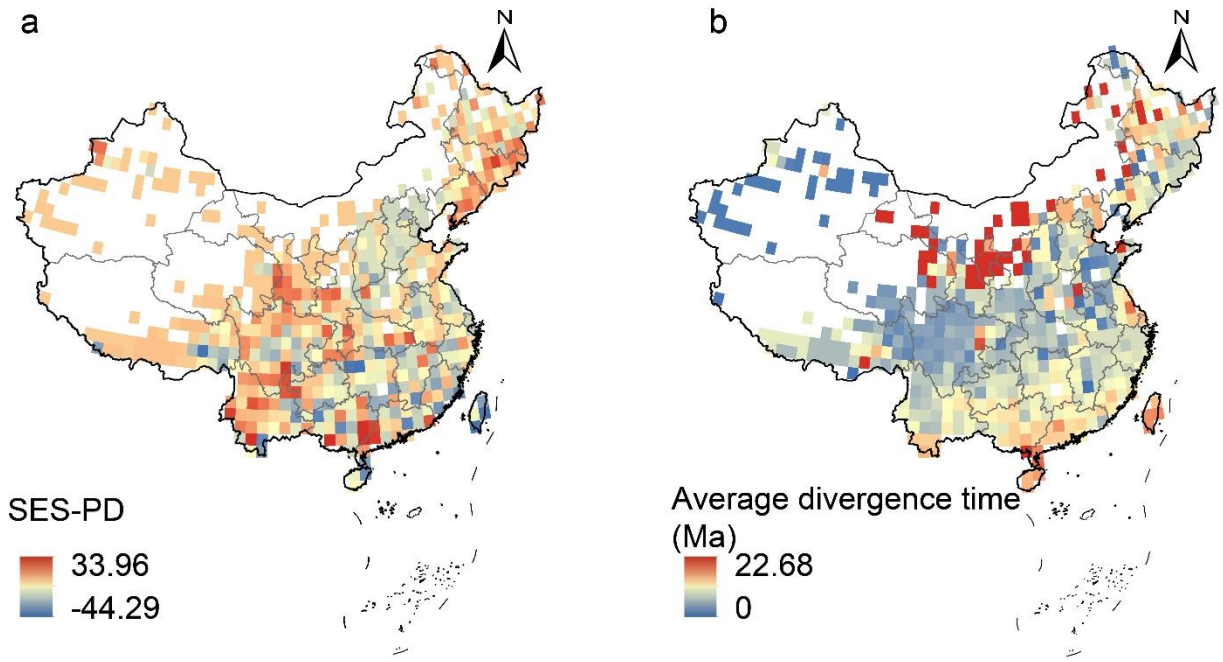

Fig. S13. Distribution among grid cells of (a) standardized phylogenetic diversity (SES-PD) and (b) average divergence time of species. SES-PD accounts for phylogenetic diversity while controlling for species richness. Higher values are indicated by darker red. The gray lines indicate the provincial boundaries of China. The average divergence time was computed as the mean value of divergence times across all species within each grid cell. To estimate this, we utilized the R package *phytools* (52). Specifically, we extracted the divergence time of each species (i.e., the time when they diverged from their sister taxon) in each grid cell, regardless of whether the sister taxon was in that grid cell. Subsequently, we summed the divergence times of all species within each grid cell and calculated the average divergence time by dividing the summed time by the species richness of that grid cell. In cases where a grid cell contained only one species, the average divergence time corresponded to the divergence time of that species. A regression analysis showed no significant relationship between these variables among grid cells (r^2<0.01; p=0.191). Analysis after correcting for spatial autocorrelation also supports the nonsignificant relationship (estimates=-0.09, z value=6.24, p=0.238). This overall result indicates that while some high-value grid cells for SES-PD and average divergence time overlap (e.g., northern China), grid cells with significantly higher SES-PD do not necessarily contain older species. Note that we did not consider either of these variables (SES-PD, mean divergence time) when delimiting hotspots, since both appear to be largely decoupled from species richness (SES-PD: r^2=0.03; p<0.001; mean divergence time: r^2<0.01; p=0.795), and our primary focus was on species richness.

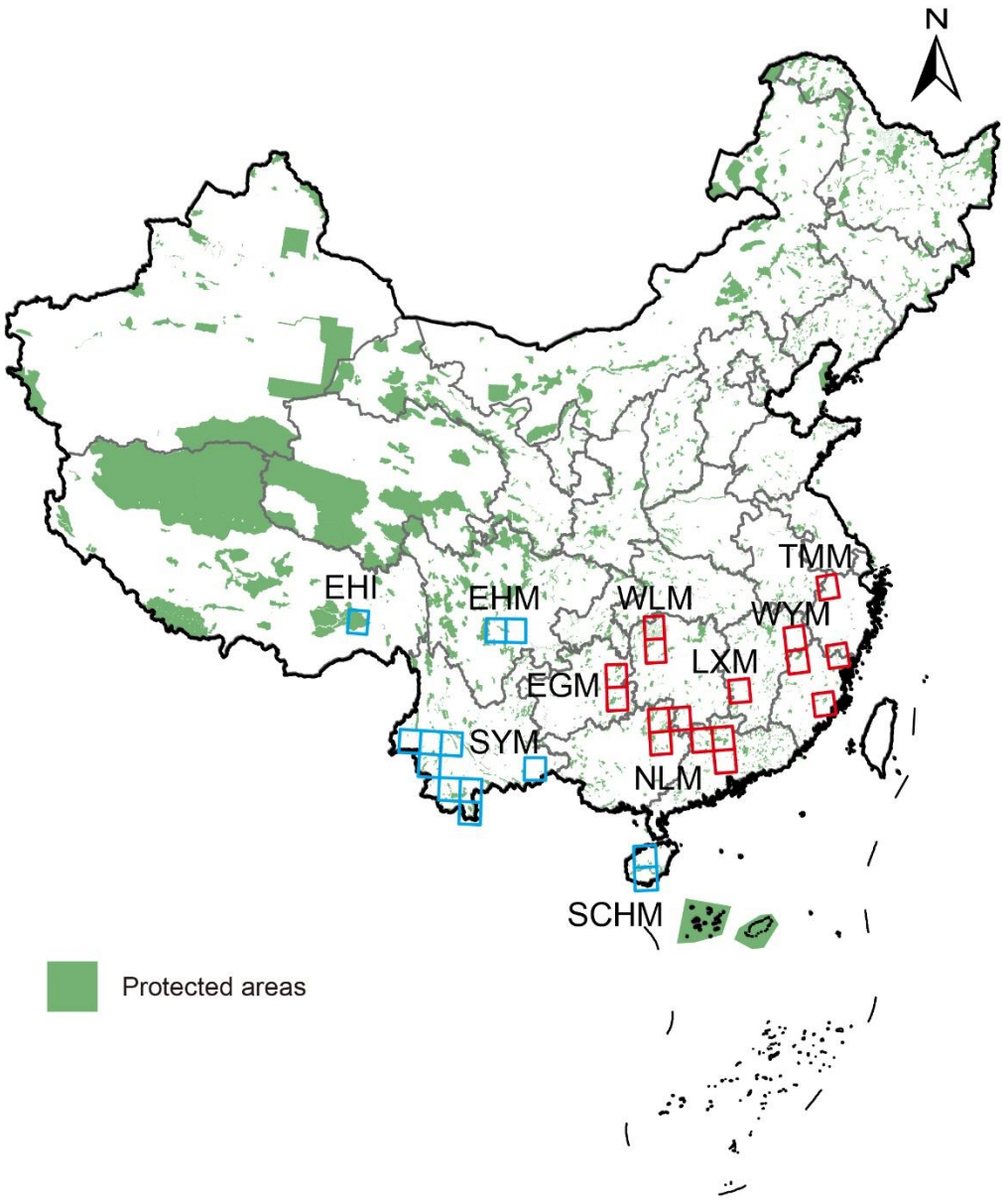

Fig. S14. Protected areas in China (green) and the location of the ten hotspots identified for Chinese amphibians. Grid cells corresponding to the six new hotspots are shown in red. Grid cells corresponding to the four old hotspots are shown in blue. Abbreviations for hotspots: EHI: Eastern Himalayas, EHM: Eastern Hengduan Mountains, SYM: Southwest Yunnan Mountains, SCHM: South-Central Hainan Mountains, NLM: Nanling Mountains, WLM: Wuling Mountains, EGM: Eastern Guizhou Mountains, LXM: Luoxiao Mountains, WYM: Wuyi Mountains, TMM: Tianmu Mountains. The gray lines indicate the provincial boundaries of China.

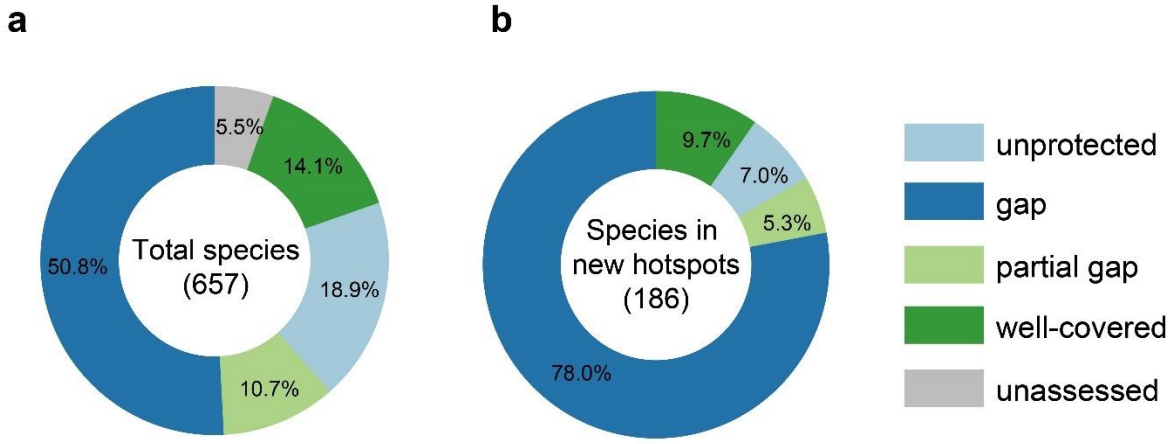

Fig. S15. The proportion of the geographic range of each species that is within protected areas. Based on the percentage of each species' range that fell inside the protected areas, we classified species into four groups: (i) unprotected: species' range was completely outside protected areas; (ii) gap: maximum of 20% covered by protected areas; (iii) partial gap: 21–90% covered by protected areas; and (iv) well-covered: >90% covered by protected areas. Species without distribution data were not assessed. Species with occurrences only in Hongkong, Macao, or Taiwan were also not assessed because of the lack of protected areas in this dataset.

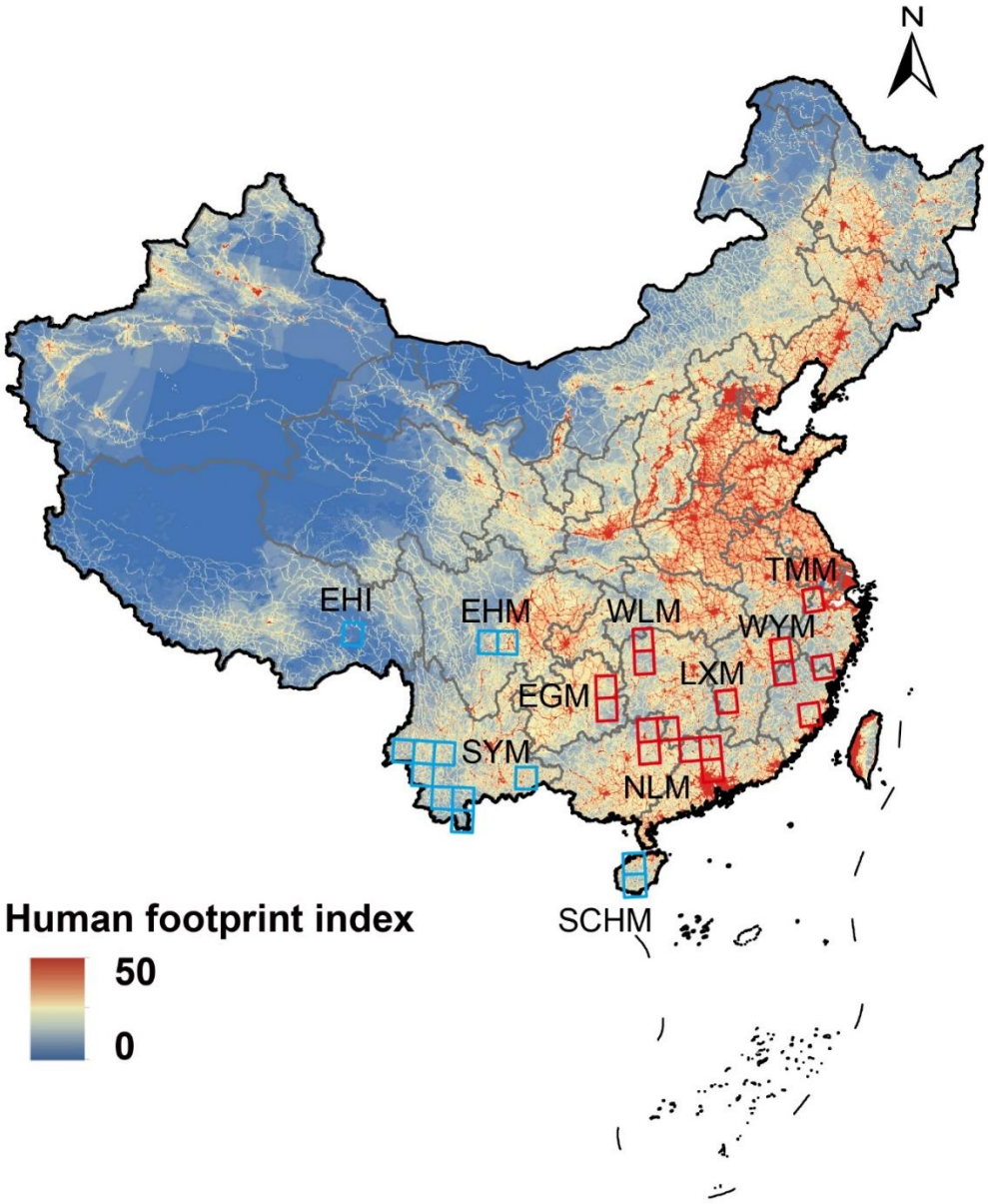

Fig. S16. Map of human footprint index and the location of the ten amphibian hotspots. Red corresponds to high human pressure, blue to low human pressure**.** Grid cells corresponding to the six new hotspots are shown in red. Grid cells corresponding to the four old hotspots are shown in blue. Abbreviations for hotspots: EHI: Eastern Himalayas, EHM: Eastern Hengduan Mountains, SYM: Southwest Yunnan Mountains, SCHM: South-Central Hainan Mountains, NLM: Nanling Mountains, WLM: Wuling Mountains, EGM: Eastern Guizhou Mountains, LXM: Luoxiao Mountains, WYM: Wuyi Mountains, TMM: Tianmu Mountains. The gray lines indicate the provincial boundaries of China.

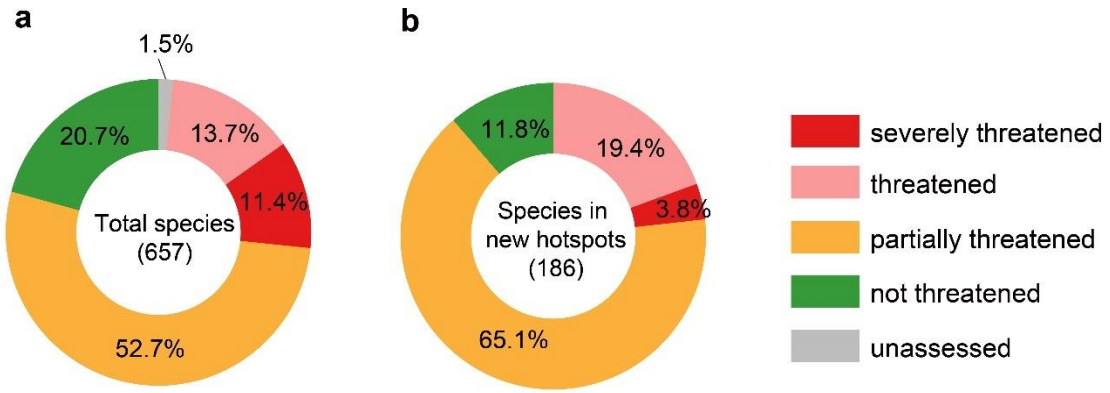

Fig. S17. Distribution of species in areas of high human pressure, for all species and those in the new hotspots. Species without distribution data were not assessed. Based on the percentage of each species' range that fell inside the high-human pressure areas, we classified species into four groups: (i) severely threatened: species' range was completely inside the very high-human pressure areas (100%); (ii) threatened: >50% in the very high-pressure areas; (iii) partially threatened: ≤50% and >0%, and (iv) non-threatened: completely outside the very high-pressure areas.

Tables S1–S5

Table S1. Summary of diversity statistics for each grid cell located in the ten hotspots. Lon=longitude of the centroid of each hotspot grid cell. Lat=latitude of the centroid of each hotspot grid cell. A "Top 5%" indicates that the total richness, endemism, phylogenetic diversity (PD), or phylogenetic endemism (PE) of this grid cell is in the upper 95th percentile among all 567 cells. Data for each grid cell is given in External Dataset S8.

Lon	Lat	Hotspots	Richness	Endemism	PD	PE
110.5	25.5	Nanling Mountains	Top 5%	Top 5%	Top 5%	Top 5%
110.5	24.5	Nanling Mountains	Top 5%	Top 5%	Top 5%	Top 5%
112.5	24.5	Nanling Mountains	Top 5%		Top 5%	
113.5	24.5	Nanling Mountains	Top 5%	Top 5%	Top 5%	Top 5%
111.5	25.5	Nanling Mountains	Top 5%			
113.5	23.5	Nanling Mountains	Top 5%		Top 5%	
108.5	26.5	Eastern Guizhou Mountains	Top 5%	Top 5%	Top 5%	
108.5	27.5	Eastern Guizhou Mountains	Top 5%		Top 5%	
114.5	26.5	Luoxiao Mountains	Top 5%	Top 5%	Top 5%	
119.5	30.5	Tianmu Mountains	Top 5%		Top 5%	
110.5	29.5	Wuling Mountains	Top 5%		Top 5%	
110.5	28.5	Wuling Mountains	Top 5%			
117.5	27.5	Wuyi Mountains	Top 5%		Top 5%	
119.5	27.5	Wuyi Mountains	Top 5%		Top 5%	
118.5	25.5	Wuyi Mountains	Top 5%			
117.5	28.5	Wuyi Mountains	Top 5%			
103.5	29.5	Eastern Hengduan Mountains	Top 5%	Top 5%	Top 5%	Top 5%
102.5	29.5	Eastern Hengduan Mountains	Top 5%	Top 5%		
95.5	29.5	Eastern Himalaya	Top 5%	Top 5%		Top 5%
109.5	18.5	South-Central Hainan Mountains	Top 5%	Top 5%	Top 5%	Top 5%
109.5	19.5	South-Central Hainan Mountains	Top 5%	Top 5%	Top 5%	Top 5%
100.5	22.5	Southwest Yunnan Mountains	Top 5%	Top 5%	Top 5%	Top 5%
104.5	23.5	Southwest Yunnan Mountains	Top 5%	Top 5%	Top 5%	Top 5%
100.5	24.5	Southwest Yunnan Mountains	Top 5%	Top 5%	Top 5%	Top 5%
99.5	23.5	Southwest Yunnan Mountains	Top 5%	Top 5%	Top 5%	Top 5%
101.5	21.5	Southwest Yunnan Mountains	Top 5%	Top 5%		Top 5%
98.5	24.5	Southwest Yunnan Mountains	Top 5%	Top 5%	Top 5%	Top 5%
101.5	22.5	Southwest Yunnan Mountains	Top 5%	Top 5%		Top 5%
99.5	24.5	Southwest Yunnan Mountains	Top 5%	Top 5%	Top 5%	Top 5%

Table S2. Summary of the proportion of protected areas and human pressures for each grid located in the ten hotspots. Lon=longitude of the centroid of each hotspot grid cell. Lat=latitude of the centroid of each hotspot grid cell. Values for the human footprint index are based on an average across ~1 km grid cells within each ~111x111 km grid cell. We followed classification of human pressure level from Venter et al. (53): no pressure, mean human footprint=0; low pressure, human footprint=1–2; moderate pressure, human footprint=3–5; high pressure, human footprint=6–11; and very high pressure, human footprint>12.

Lon	Lat	Hotspots	Proportion of protected areas	Human footprint index	Human pressure level
110.5	25.5	Nanling Mountains	11.14%	7.25	high pressure
110.5	24.5	Nanling Mountains	11.11%	7.30	high pressure
113.5	24.5	Nanling Mountains	17.57%	10.26	high pressure
111.5	25.5	Nanling Mountains	5.87%	11.26	high pressure
112.5	24.5	Nanling Mountains	11.53%	14.00	very high pressure
113.5	23.5	Nanling Mountains	1.96%	18.85	very high pressure
108.5	26.5	Eastern Guizhou Mountains	8.35%	7.30	high pressure
108.5	27.5	Eastern Guizhou Mountains	10.87%	9.25	high pressure
114.5	26.5	Luoxiao Mountains	6.78%	7.25	high pressure
119.5	30.5	Tianmu Mountains	1.56%	7.25	high pressure
110.5	28.5	Wuling Mountains	8.19%	6.58	high pressure
110.5	29.5	Wuling Mountains	5.46%	11.03	high pressure
117.5	27.5	Wuyi Mountains	10.27%	6.26	high pressure
119.5	27.5	Wuyi Mountains	5.32%	12.00	very high pressure
117.5	28.5	Wuyi Mountains	0.44%	14.85	very high pressure
118.5	25.5	Wuyi Mountains	4.41%	16.00	very high pressure
102.5	29.5	Eastern Hengduan Mountains	18.12%	6.32	high pressure
103.5	29.5	Eastern Hengduan Mountains	2.09%	18.75	very high pressure
95.5	29.5	Eastern Himalaya	61.66%	1.59	low pressure
109.5	18.5	South-Central Hainan Mountains	8.88%	11.50	high pressure
109.5	19.5	South-Central Hainan Mountains	7.35%	13.23	very high pressure
100.5	22.5	Southwest Yunnan Mountains	11.41%	5.46	moderate pressure
98.5	24.5	Southwest Yunnan Mountains	1.43%	6.37	high pressure
99.5	24.5	Southwest Yunnan Mountains	4.10%	7.25	high pressure
100.5	24.5	Southwest Yunnan Mountains	7.84%	7.75	high pressure
101.5	21.5	Southwest Yunnan Mountains	15.05%	8.50	high pressure
104.5	23.5	Southwest Yunnan Mountains	1.51%	9.23	high pressure
99.5	23.5	Southwest Yunnan Mountains	8.79%	10.32	high pressure
101.5	22.5	Southwest Yunnan Mountains	9.17%	13.00	very high pressure

Table S3. The optimal partitioning scheme and best-fit model determined by IQ-TREE for all the partitions. We provided IQ-TREE with initially defined data blocks corresponding to three codon positions for each protein-coding gene and the full length for ribosomal genes (12S and 16S rRNA). Data blocks that had the same best-fit model, as determined by IQ-TREE, were grouped into the same partitions. IQ-TREE includes all commonly used DNA models, such as GTR, JC, HKY, TIM, and others. Notably, the "2" in TIM2 refers to an extension of the TIM model that explicitly models AC=AT, CG=GT, and unequal base frequencies. The "e" in TIMe denotes a similar model as TIM but with equal base frequencies. "F" indicates empirical base frequencies. "I" refers to the inclusion of invariant sites in the substitution model. "G" refers to the inclusion of a gamma distribution of rates among sites in the substitution model. "R" indicates a model that generalizes the G model by relaxing the assumption of gamma-distributed rates. This free-rate model typically fits the data better than the G model and is recommended for analysis of large data sets (54). The number associated with G (e.g., G4) specifies the number of rate categories in the gamma distribution and was determined automatically by IQ-TREE. A higher number of rate categories allows for a more fine-grained description of rate variation among sites. The number associated with "R" specifies the number of estimated base frequencies. For example, R4 means that the model estimates the base frequencies using four free parameters. ASC indicates the ascertainment bias correction model.

Partition	Best-fit model
12S rRNA, 16S rRNA	GTR+F+R10
bdnf_codon1, pomc_codon3	TIM2+F+I+G4
bdnf_codon2	K2P+R3
bdnf_codon3	TIM2e+R4
cmyc_codon1	TIMe+I+G4
cmyc_codon2	HKY+F+I+G4
cmyc_codon3	GTR+F+G4
coi_codon1	GTR+F+R9
cxcr4_codon2, rhod_codon2	TVM+F+R4
coi_codon2	K3Pu+F+R4
coi_codon3	TIM2+F+R7
cxcr4_codon1	TVMe+I+G4
cxcr4_codon3, h3a_codon1	GTR+F+I+G4
cytb_codon1, nd1_codon1	SYM+R7
cytb_codon2	GTR+F+R5
nd2_codon3, rag1_codon2	GTR+F+R6
cytb_codon3	GTR+F+R7
h3a_codon2	JC+R2
h3a_codon3, rag2_codon2	TVM+F+G4
ncx1_codon1, slc8a_codon1	GTR+F+R4
ncx1_codon2	TVM+F+R3
ncx1_codon3, pomc_codon1	TVM+F+I+G4
nd1_codon2	TVM+F+R6

nd1_codon3	TIM2+F+R8
nd2_codon1	TIM2+F+R6
nd2_codon2	GTR+F+R8
nd3_codon1	TIM2+F+R5
tyr_codon1, rhod_codon1	SYM+I+G4
nd3_codon2	TPM2+F+R5
pomc_codon2, rag2_codon3, nd3_codon3	TIM3+F+I+G4
rag1_codon1	TVMe+R5
rag1_codon3	K3Pu+F+I+G4
rhod_codon3	TIM2+F+G4
rag2_codon1	TIM2e+G4
sia_codon1	SYM+R3
sia_codon2	JC
sia_codon3	TN+F+I+G4
slc8a_codon2	K3Pu+F+R2
slc8a_codon3	TPM2+F+R4
tyr_codon2	SYM+R4
tyr_codon3	TIM2e+R6

629

Table S4. Number in each category of species based on the species delimitation analyses, total number of described species by the end of 2020, and total number of species involved in the species delimitation analyses. The number of cryptic species is the minimum number of cryptic species inferred among the three methods. Cryptic species retrieved from published studies (External Dataset S2) were also included here.

Family	Species identification suggestions			Described species	Total species
	Match	Merge	Cryptic species		
Bombinatoridae	0	0	0	5	8
Bufonidae	9	0	6	15	30
Ceratobatrachidae	1	0	0	4	4
Dicroglossidae	10	0	3	38	80
Hylidae	2	1	0	8	20
Hynobiidae	11	0	0	28	42
Ichthyophiidae	1	0	0	1	11
Megophryidae	94	0	56	117	199
Microhylidae	3	2	1	17	49
Ranidae	54	7	12	115	196
Rhacophoridae	32	2	10	65	95
Salamandridae	21	2	6	40	47
Cryptobranchidae	---	---	6	---	---

Table S5. Species richness of each biogeographic region delimited for Chinese amphibians. Corrected richness is the total species richness of a region divided by the number of grid cells in the region.

Biogeographic regions	Number of grid cells	Total richness	Corrected richness
South China	195	422	2.2
South Yunnan Mountains	9	105	11.7
Yunnan Plateau	26	129	5.0
North China	190	44	0.2
Qinghai-Xizang Plateau	68	50	0.7
Himalayas	4	40	10.0
Hengduan Mountains	10	23	2.3
Northwest China	37	5	0.1